Article

Comparative Evaluation of the Shear Adhesion Strength of Ice on PTFE Solid Lubricant

Emad Farahani [1], Andre C. Liberati [1], Christian Moreau [1], Ali Dolatabadi [2] and Pantcho Stoyanov [3,*]

[1] Department of Mechanical, Industrial and Aerospace Engineering, Concordia University, Montreal, QC H3G 1M8, Canada
[2] Department of Mechanical and Industrial Engineering, University of Toronto, Toronto, ON M5S 3G8, Canada
[3] Department of Chemical and Materials Engineering, Concordia University, Montreal, QC H3G 1M8, Canada
[*] Correspondence: pantcho.stoyanov@concordia.ca

Abstract: The development of a durable and green icephobic coating plays a vital role in the aviation industry due to the adverse impact of ice formation on aircraft performance. The lack of study into how temperature and surface roughness impact icephobicity is the main problem with present icephobic coatings. This study aims to qualitatively evaluate the icephobicity performance of a polytetrafluoroethylene (PTFE) solid lubricant film, as an environmentally friendly solution, with a custom-built push-off test device in different icing conditions utilizing a wind tunnel. The ice-adhesion reduction factor (ARF) of the film has been assessed in comparison to a bare aluminium substrate (Al 6061). The impact of surface energy was investigated by comparing the water contact angle (WCA), the contact angle hysteresis (CAH), and the pull-off force of the PTFE solid lubricant and Al with an atomic force microscope (AFM). The results of ice shear adhesion on the PTFE solid lubricant film showed a significant reduction in the ice adhesion force at various substrate temperatures and surface roughness compared to the bare aluminium substrate. The difference in the ice adhesion between the solid lubricant and aluminium alloy was attributed to the differences in the detachment mechanism. For the PTFE-based solid lubricant, the interfacial detachment mechanism was based on the formation of interfacial blisters towards the centre of the ice. Consequently, upon continued application of the shear force, most of the energy injected would be distributed throughout the blisters, ultimately causing detachment. In the comparison of ice adhesion on PTFE solid lubricant and bare aluminium, the film showed minimal ice adhesion at −6 °C with an adhesion force of 40 N (ARF 3.41). For temperature ranges between −2 °C and −10 °C, the ice adhesion for bare aluminium was measured at roughly 150 N.

Keywords: shear strength; ice adhesion; PTFE solid lubricant; roughness; temperature

1. Introduction

Ice formation can negatively affect the structural integrity and performance of components during service in many fields [1]. In the aviation industry, the ice formation phenomenon occurs when supercooled water droplets exist in certain conditions and freeze upon impact on the surface of an aeroplane. Based on the published literature, an ice layer can cover aerodynamic sections of an aircraft, subsequently resulting in increased fuel consumption, harmful vibrations, reduced lift, and increased drag. As a result, developing anti-icing technologies and systems to avoid, or at least minimize, the ice adhesion is essential [2,3].

To address these issues, the aerospace industry employs various passive anti-icing methods and active de-icing methods to prevent or minimize ice formation before and during flights, respectively, [4,5]. The use of durable icephobic coatings as a passive method may be more trustworthy from an economic and environmental standpoint. Despite multiple attempts to employ hydrophobic or icephobic coatings, the mechanical durability

of passive coatings or their anti-icing performance may be reduced after several icing/de-icing cycles [6,7]. Some researchers evaluated durability by melting the ice, followed by measuring the water contact angle (WCA) and contact angle hysteresis (CAH) [8], while the ice adhesion was not measured after de-icing cycles. In addition, others evaluated the performance of their coatings at a specific temperature [9], for specific roughness [10], or with an icing condition that generates a particular type of ice [11].

Due to their hydrophobicity and water repellency, polymers are among the elements utilized for developing icephobic coatings [12,13]. For example, low-modulus elastomers were shown to be inherently icephobic [14], and it has been reported that polymer-lubricated systems have relatively low ice adhesion strengths, reduced wettability, and delayed freezing times [15,16]. The bulk of composite coatings were prepared using some organic solvent, which significantly accelerated the pollution of the environment. To reduce energy consumption and environmental damage, it is especially important to look for a clean, alternative energy source to replace the use of organic solvents [17]. However, among different polymers that can be used as an ice-repellent surface, polytetrafluoroethylene (PTFE) provides additional advantages, such as environmentally friendly and non-toxicity properties [18], low surface energy, excellent hydrophobicity, and high water-repellency due to its CF2 group [19]. These advantages make PTFE an attractive and trustworthy choice for developing icephobic coatings [19–21]. Some studies have also used solid lubricants or PTFE as an infusion into a textured substrate and evaluated the anti-icing and water-repellency properties [22,23]. Using PTFE as a lubricant on porous surfaces has been shown to result in a SLIPS (slippery liquid-infused porous surface) that helped reduced ice adhesion on a polymer surface [24–26] while providing enough adhesion between polymer and substrate. Chien et al. [27] employed PTFE as the main colloidal material in a "polymeric micelle dispersion" with polydimethylsiloxane (PDMS). After heating the applied coating to remove the water solvent, two more oil-infused layers were added to protect and increase the lifetime of the coatings. Another study showed a reduction in ice adherence by coating an Al substrate with a PTFE nanostructure while only measuring an ice adhesion of 320 kPa at −10 °C with a very low wind speed of 10 m/s [20].

A solid lubricant is a substance applied as a powder or thin layer that reduces wear and friction on contacting surfaces while moving relative to one another. Solid lubricants based on PTFE are also well known for their very low static coefficient of friction to their lamellar structure [28]. The PTFE solid lubricant film is a solvent-based composite of PTFE with a polyamide-imide binder. The structure of PTFE solid lubricant is made by a polymerizing chain of tetrafluoroethylene molecules consisting of a crystalline fluoropolymer with a long parallel macro-molecule. Each chain is made of two carbons surrounded by four fluorine atoms, where fluorine atoms with high electronegativity make a strong bond with carbon in one CF2 group. Since forces in CF2 are not polarizable, and its surface energy is low, high hydrophobicity and an effective lubricant are obtained [29,30]. Similar to the hexagonal planes of solid lubricants with lamellar structures, very weak van der Waals interactions form between neighbouring PTFE molecules, allows them to move freely past one another at low shear stresses. Therefore, this polymer-based solid lubricant could be an excellent choice to reduce ice adhesion [31]. The non-toxic properties of PTFE and the binder of this solid lubricant could make it a sustainable option to reduce adhesion while preserving the environment [17,18].

To thoroughly assess the icephobic characteristic of a coating, two methods for forming ice have been used. First, static icing inherently suffers from the lack of realistic representation of natural ice production [31]. Second, an icing wind tunnel (IWT) can be leveraged to mimic real in-flight icing in an adjustable and well-controlled manner [32]. However, icing parameters, such as water droplet velocity, size, and test section temperature, can all affect ice adhesion measurement results [33,34].

While ice-forming methods are relatively straightforward, the precise measurement of ice adhesion is not and hence is actively researched. It is known that variations in adhesion measurement methods, such as shear, tensile, or centrifugal, can be attributed to testing

circumstances, e.g., temperature, surface characteristics, ice type, and icing factors [11,35]. The shear strength method has received a surge of interest among ice adhesion measurement methods since it can replicate the wind drag force needed to remove the ice [33]. Adhesive shear strength measured by this method is more concerned with the interlocking mechanism, which is affected by several factors, such as roughness, surface temperature, and actual contact area at the ice–solid interface [36]. Although researchers have attempted to minimize unknown variables as much as possible, conducting a comparative study on the results of ice shear strength is a complex and challenging task, and a research gap exists in developing a standard test procedure for ice adhesion measurements.

The primary goal of this research is to critically evaluate PTFE solid lubricants in terms of their ice adhesion behaviour. The shear adhesion strength of the ice was tested using custom-built test equipment, while the ice was developed utilizing an IWT to simulate in-flight icing. Following the anti-icing performance evaluation, the ice adhesive shear strength on PTFE solid lubricants was compared with the bare Al 6061 substrate at various temperatures and for different surface roughness.

2. Experiments

2.1. Sample Preparation

A PTFE solid lubricant film (Everlube® R75, Everlube, Peachtree City, GA, USA) was applied onto a substrate of Al 6061 (McMaster, Hamilton, ON, Canada), of dimensions 20 mm × 40 mm × 10 mm. Bare Al 6061 of the same dimensions was also taken as a reference for comparison.

The Al 6061 samples were polished using SiC paper or sandblasted using aluminium oxide particles (Trinity Tool Company, Fraser, MI, USA) to examine the effect of icing temperature on ice adhesion. The final roughness of the Al samples was approximately 1 ± 0.2 µm. As a substrate for applying the PTFE solid lubricant, other Al samples were polished without sandblasting (Ra = 0.6 ± 0.05 µm). All samples were cleaned in an ultrasonic bath for ten minutes, then dipped in distilled water and ethanol before being air-dried to eliminate any remaining contamination. The PTFE solid lubricant was applied to the Al substrate using a brush and then cured for 12 h in air. The final film had a roughness of approximately 1 ± 0.1 µm and a thickness of around 25 ± 5 µm (as determined by a digital film thickness gauge).

In another part of the experiment, three bare Al 6061 samples were prepared to assess the effect of roughness on ice adhesion at −10 °C. The first Al sample was polished to create an average roughness of 0.3 ± 0.05 µm, and the second sample was sandblasted using aluminium oxide, which resulted in an average roughness of 1 ± 0.2 µm; both served as the reference for the adhesion measurements. The third Al sample, which had been polished to an average roughness of 0.6 ± 0.05 µm, was then used to apply the PTFE solid lubricant film by brushing and dipping, resulting in final average roughness values of 0.3 ± 0.03 µm and 1 ± 0.1 µm, respectively.

2.2. Surface Analysis

A confocal laser microscope (LEXT OLS 4100, Olympus Corporation, Tokyo, Japan) was used to capture surface images and investigate the surface properties of PTFE solid lubricant and Al. Cryogenic SEM/Confocal equipment, which was required to examine the ice surface, was unavailable. This equipment was used to analyse roughness parameters on 2 mm × 2 mm areas per ISO 4288 and ISO 25178-3 [37]. In addition to the average roughness (R_a), other roughness characteristics are important determinants for atmospheric icing, which might impact the mechanical interlocking and interfacial mechanism [20,36]. Therefore, several roughness metrics, such as root-mean-square roughness (R_q), skewness coefficient (R_{sk}), and kurtosis (R_{ku}), were also measured to have a better understating of their effect on ice adhesion.

Surface roughness can be represented by R_a and R_q. R_a, is determined as the average of profile heights and depth deviations from the mean line. By definition, the root-mean-

square (RMS) roughness, R_q, includes R_a and the standard deviation of the roughness ($R_q{}^2 = R_a{}^2 + \sigma^2$), which provides more information on the variation of the surface profile heights. A measurement of the asymmetry of the profile around the mean line is the skewness on the surface or R_{sk}: negative skewness values indicate more valleys, whereas positive values indicate more peaks. Kurtosis, R_{ku}, is a metric for determining how peaked or flat a profile is; a value of three implies a normal (Gaussian) distribution of peaks and valleys throughout the surface of the sample. $R_{ku} > 3$ indicates that the surface has sharper peaks, while $R_{ku} < 3$ indicates that most of the surface peaks are skewed and it has rounded peaks [38].

The pull-off force on the bare Al and the PTFE solid lubricant surfaces was measured at the nanoscale. This measurement was performed in tapping mode using an atomic force microscope (AFM, Tosca 400, Anton Paar, Graz, Austria), with a tip size of 5–10 nm interacting with the surface. The pull-off force is determined by the work of adhesion, which is defined as the work per unit area necessary to separate two perfectly flat bodies reversibly. The work of adhesion (also known as the Dupré energy of adhesion) is proportional to the surface energies of the contacting substances [39].

Additionally, the WCA and CAH were measured for the PTFE solid lubricant and Al to indicate surface wettability. The CAH represents the difference between the advancing and receding angle of a water droplet on a surface. This evaluation was performed using the sessile droplet method at room temperature and humidity [40]. The WCA helps to determine the static wettability of a solid surface, while the CAH is an indication of water mobility on the surface [41]. For this purpose, a dispenser was used to form 10 μL water droplets from deionized water. These droplets were placed on the surface with zero velocity. The WCA and CAH testing images were captured with a high-speed camera (Photron Ltd., Tokyo, Japan) with a backlight LED. Then, the DropSnake plugin of ImageJ software was used to calculate the values of WCA and CAH [42]. Furthermore, the surface temperature was monitored using an infrared (IR) camera (A320 Thermo Vision, FLIR System) before and during the ice formation.

2.3. Ice Development Process

An IWT was utilized to form the ice on Al and the PTFE solid lubricant samples. The wind tunnel performance is discussed in more detail in other studies [43,44]. To summarize, samples installed in the test section have a dimension of 33 mm × 10.2 mm ×10.2 mm. Supercooled water droplets were generated by spraying deionized water (Spraying Systems Company, Mississauga, ON, Canada). These droplets impacted the sample surface at 90°, interacted with different surface asperities, and froze upon impingement.

A thermocouple was mounted behind the sample in the test section to continuously measure the temperature of the test section without impacting the ice formation process. After roughly 40 trial runs, the icing parameters were narrowed down to obtain a 2–3 mm thickness of the most consistent ice shape on the surface, as shown in Table 1. As the icing conditions of the IWT remained constant, the produced chunk of ice had the same thickness and shape for both the Al and PTFE solid lubricant films. In assessing the temperature impact on ice adhesion, the IWT parameters were held constant except for temperature, consequently producing clear, mixed, and rime-mixed ice. It is important to mention that the temperature was fixed at −10 °C in the second section to evaluate the roughness effect. The liquid water content (LWC) is a measure of humidity expressed as the mass of water in one cubic meter and it was determined by balancing the mass flow rate of water droplets between the outlet of the spray nozzle and the test section with the mentioned dimensions [43]. The median volumetric diameter (MVD) of water droplets was measured using a laser diffraction system (SprayTech system, Malvern Panalytical Ltd., Malvern, UK).

Table 1. Icing wind tunnel parameters.

Temperature (°C)	Airspeed (m/s)	MVD (µm)	LWC (gr/m^3)	Ice Type
0 to −3	45 ± 3	20 ± 3	0.2 ± 0.02	Clear or Glaze
−3 to −6	45 ± 3	20 ± 3	0.2 ± 0.02	Mixed
−7 to −10	45 ± 3	20 ± 3	0.2 ± 0.02	Rime-mixed

Since temperature variations may change the properties and type of ice, the icing temperature, the temperature in which the substrate and test section are in equilibrium, has been identified as a factor that significantly affects ice adhesion [45,46]. This icing temperature leads to the generation of various types of ice. Clear ice, or glaze ice, refers to a sort of ice that is mostly smooth, transparent, and very adherent to the surface. Clear ice formation occurs when the temperature is usually near zero. Droplets of supercooled water hit the surface but do not instantly and entirely freeze upon impact and spread across the surface while maintaining the liquid state. The liquid droplets will diffuse into the asperities of the surface after impact and can make strong bonds with the valleys and peaks of the surface, resulting in strong mechanical interlocking. On the other hand, by lowering the temperature gradually, mixed ice (−3 to −6 °C), rime-mixed ice (−7 to −10 °C), and fully rime ice (−20 °C) can develop, and each of these has different strengths and structures compared to clear ice [46,47]. In the case of mixed or rime ice, the droplets instantly solidify upon impact, entrapping air pockets that lead to several internal flaws and a relatively weaker structure [48,49]. It has been shown that mixed ice can have a larger grain size with lower strength, but rime-mixed has a smaller grain with higher strength [50]. However, due to limitations of the IWT of this study (minimum icing temperature of −10 °C), the production of rime ice was not observed. It is also worth noticing that this minimal temperature of −10 °C, obtained at the wind tunnel's highest speed of 45 m/s, may induce limitations when compared to standard in-flight conditions.

2.4. Measurement of Ice Shear Strength

A custom-built instrument (Figure 1) was used to assess interfacial fracture in shear. A motorized linear stage moving at a constant speed of 0.5 mm/s was equipped with a force gauge (NEXTECH, DFS-1000 series) with a precision of 0.1 N. The threshold sliding velocity at which abrupt de-bonding occurs at high loads was kept constant to control the strain rate [51]. The force was supplied to the ice around 1 mm above the interface to achieve pure shear stress [52]. The Nex-Graph software was used to capture force data as a function of time, and the maximum force at the instant the ice detached was noted as the maximum adhesive shear force. It is challenging to compare ice adhesion results between different studies since most researchers did not mention some crucial factors, such as roughness, substrate temperature, and the speed of the shear test rig [10]. However, the adhesion reduction factor (ARF) was used in this study as a factor that was calculated by dividing the ice adhesion on bare aluminium by ice adhesion on the target coating, $\tau_{Al}/\tau_{coating}$. It has been reported as a more reliable comparative method to show the anti-icing performance of the coatings [11].

The adherence of ice to a substrate may be controlled by several mechanisms at the interface. Most currently accepted mechanisms rely on the mechanical and physical characteristics of the coating, such as its elastic modulus [53]. Since the mechanism of ice/solid lubricant films has never been analysed, it is crucial to assess what happens at the interface to fully understand the effect of a PTFE solid lubricant film on ice adhesion reduction. To this effect, a high-speed camera (Photron Ltd., Tokyo, Japan) equipped with a wide-angle lens was used to image the interfacial fracture through clear ice.
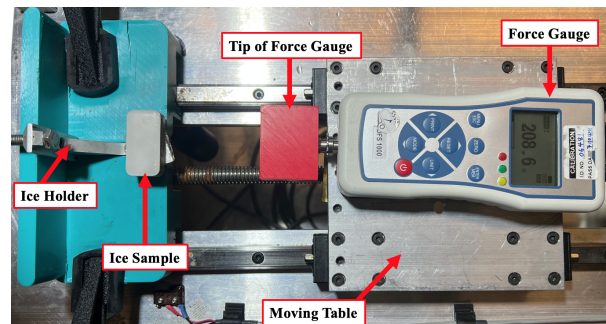
Figure 1. Details of custom-built ice shear adhesion test apparatus.

The tests were conducted according to the following steps to ensure reproducibility. First, pre-cooled samples were placed inside the IWT at a specific icing temperature to ensure the test section and surface temperatures were in equilibrium. Second, the ice was developed on the samples for three minutes, resulting in a block of ice with approximately 2–3 mm thickness. Then, the ice sample was removed from the IWT and installed in the push-off test rig in less than 30 s. Finally, the ice was detached using the force gauge, and the required maximum force was measured. This procedure was repeated nine times for each sample.

3. Results

3.1. Surface Analysis

The results of the pull-off force (i.e., by means of AFM), WCA, and CAH for Al and the PTFE solid lubricant are listed in Table 2. As observed from Table 2, the Al surface exhibited a static WCA of 62°, which was less than the WCA of the PTFE solid lubricant (94°). Furthermore, the CAH of the PTFE solid lubricant was equal to 48°, lower than Al, which had a CAH of 83°. A surface with a lower WCA and higher CAH, such as Al, is known as hydrophilic and is known to have higher surface energy and a higher wettability [54].

Table 2. Results of surface energy analysis.

	Pull-Off Force (µN)	WCA (°)	CAH (°)
Aluminium	0.182 ± 0.8	62 ± 5	83 ± 4
PTFE	0.105 ± 0.01	94 ± 2	48 ± 6

The pull-off force of Al was measured at 0.182 µN by means of AFM, which was 45 percent higher than that of the PTFE solid lubricant film. This force is proportional to the surface energy or surface tension, as expressed in Equation (1) [55]:

$$F_{ad} = \frac{3}{2} \frac{R_1 \times R_2}{R_1 + R_2} \pi W \tag{1}$$

where F_{ad} represents the adhesion force between two bodies in contact with radius R_1 and R_2, and W is the free surface energy change of two surfaces in adhesive contact [55]. Studies have shown that a reduction in nanoscale adhesion can be appropriately related to the lower surface energy of the surface since the effective radius is the same [39]. As a result, the decreased pull-off force on the PTFE solid lubricant surface (Table 2) validated its lower surface energy. It should be noted that the surface temperature was measured using an IR camera during the icing experiments, and the results indicated that the PTFE solid lubricant took 325 s to reach −1 °C, whereas the bare surface reached such a temperature in 140 s. These results may suggest that the droplets did not instantly freeze upon impact, giving them additional time to remain liquid on the surface of the PTFE solid lubricant at lower temperatures (e.g., between 0 °C and −6 °C). It has been demonstrated that a decrease in

heat transmission and the probability of heterogeneous ice nucleation can contribute to ice nucleation delay [56].

3.2. Shear Strength Adhesive Testing

Figure 2 illustrates the detachment of the ice from the bare Al during the shear force adhesion test. These images were taken with increasing time and force. The white arrows show where the shear force was applied to the length of the sample from above, and the green arrows show where cracks appeared. In the initial step, the ice did not present any specific defects and appeared to be quite homogeneous (Figure 2a), but a crack was initiated at the ice and Al interface as soon as the shear force was increased (Figure 2b). The initial crack eventually propagated to the ice surface, and a second crack appeared at the interface on the corner of the sample (Figure 2c). Eventually, the ice broke into multiple pieces through cohesive failure (Figure 2d), and after final detachment, no segment of ice remained on the substrate (Figure 2e). It was observed that cracks started at the interface but propagated within the ice with increasing shear force.
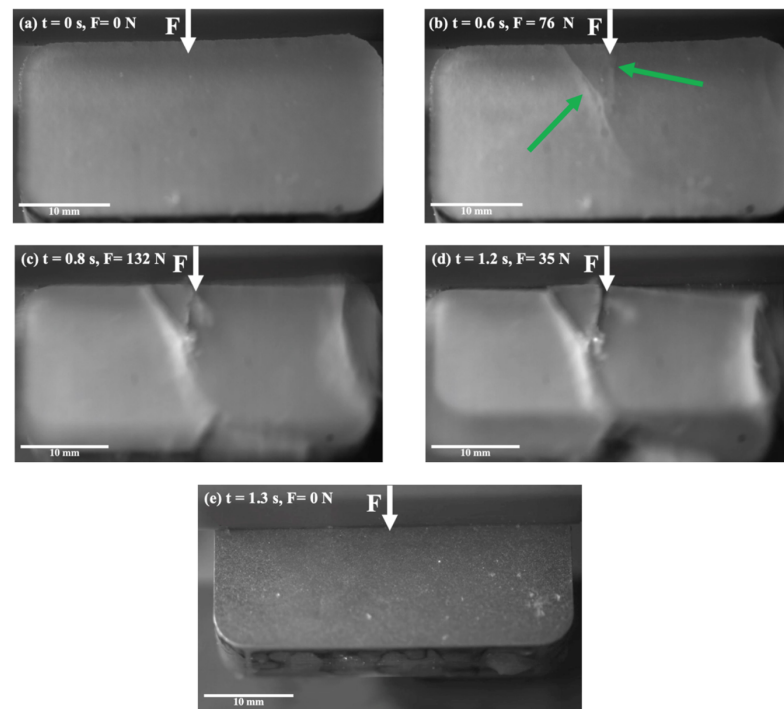

Figure 2. Snapshots from the ice shear strength testing on the Al substrate, at −2 °C.

On the other hand, a different behaviour was observed during the ice detachment on the PTFE lubricant at −2 °C, as compared to the one observed for Al in Figure 2. Figure 3 illustrates the surface of the ice during the detachment from the PTFE solid lubricant over time. The shear force was applied to the length of the sample from above, as indicated by the white arrows, and blisters are shown by the green arrows. Figure 3b shows the appearance of some blisters at the interface of PTFE solid lubricant and ice at the centre of the sample immediately after applying the force. As the force increased, another blister gradually appeared at the interface (Figure 3c), and existing blisters started to grow (Figure 3d). By increasing the force, the number of blisters increased at the interface centre, and existing blisters expanded further in the direction of applied force (Figure 3e). Finally, the developed blisters propagated along the interface towards the edges, and the ice was detached from the surface without breaking (Figure 3f).

Figure 4a–c show the initiation of blistering during the ice shear strength testing on the PTFE solid lubricant at different icing temperatures. At −2 °C, fairly small and circular blisters were observed at relatively low forces (25 N) (Figure 4a). At −6 °C, larger blisters appeared

at lower forces (10 N) (Figure 4b). Finally, at −10 °C, narrowly shaped blisters appeared at much higher shear strengths than for the previous temperatures (95 N) (Figure 4c).
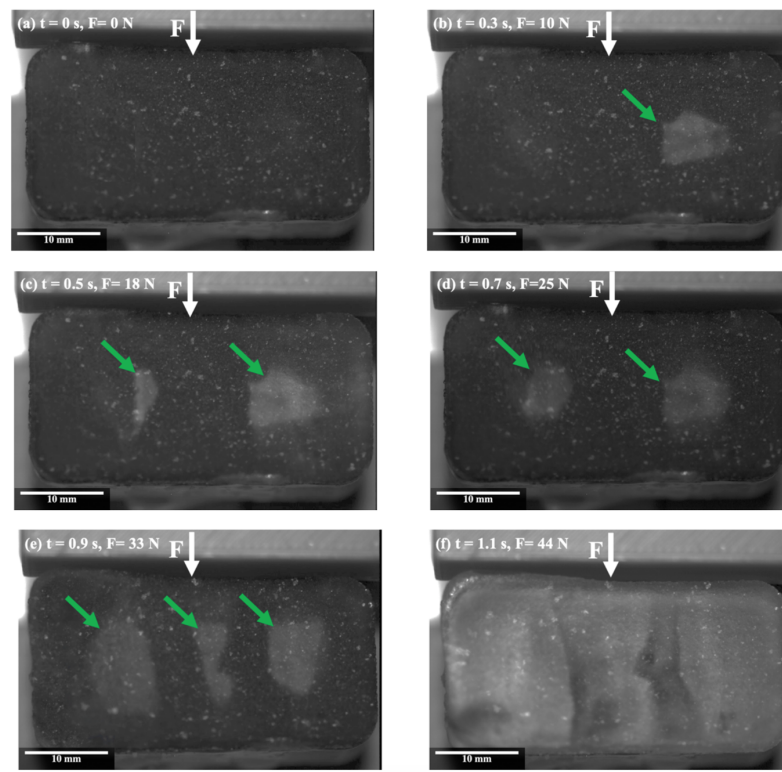

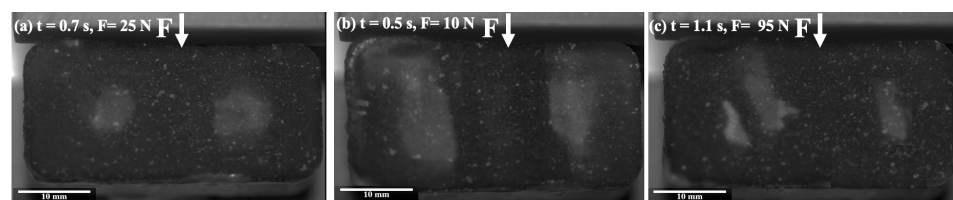**Figure 3.** Snapshots from the ice shear strength testing on the PTFE solid lubricant, at −2 °C.

Figure 4. Images of the initiation of blistering during ice shear strength testing on the PTFE solid lubricant, at several icing temperatures (**a**) −2 °C, (**b**) −6 °C, and (**c**) −10 °C.

3.3. Effect of Temperature on Ice Adhesion

To evaluate the effect of temperature on ice adhesion, the results of maximum shear adhesive force as a function of icing temperatures (from −2 °C to −10 °C) for bare Al and the PTFE solid lubricant are shown in Figure 5: the error bars correspond to the standard deviation of the nine measurements that were performed. As shown in Figure 5, it can be observed that the maximum shear force required to remove the ice from the PTFE solid lubricant was lower than on the bare Al for all temperatures. At −2 °C, the maximum shear force for ice detachment on the Al surface was near the highest obtained for Al (160 N). For intermediate temperatures (−3 °C to −6 °C), a slight decrease in adhesion strength was observed (<150 N), with a minimum of 120 N measured at −3 °C. Finally, for lower temperatures (−7 °C to −10 °C), adhesion remained relatively constant at around 170–180 N. On the other hand, the adhesive shear force of ice on the PTFE solid lubricant was considerably lower at −2 °C, measured at half the adhesive shear force of Al (80 N). With decreasing temperature, a minimal force of 40 N was obtained at −6 °C. As with the adhesive force on the bare Al substrate, further decreasing the temperature (from −7 °C to −10 °C) resulted in a steady increase in the ice adhesion shear force of the PTFE solid lubricant, up to 140 N at −10 °C, which is quite close to the force of the bare Al substrate.
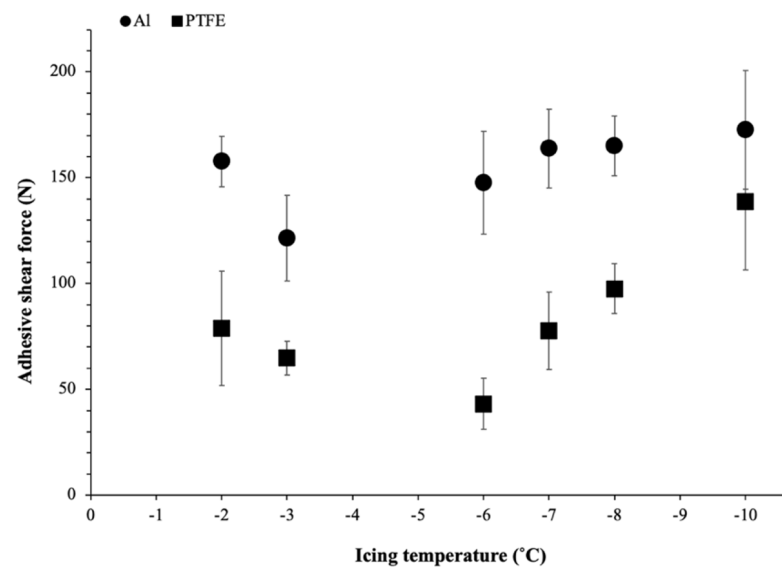
Figure 5. Ice adhesion shear force measured on bare Al and the PTFE solid lubricant for different icing temperatures.

The ARF may be used as a comparative tool to identify icephobicity and characterize how effectively the PTFE solid lubricant performed to minimize ice adhesion. The values of ARF at different icing temperatures have been calculated and are shown in Table 3. An ARF around 2 was calculated for temperatures of -2 °C and -3 °C. The lowest ice adhesive force on the PTFE solid lubricant obtained at -6 °C resulted in a maximal ARF value of 3.41. Finally, after reducing the freezing temperature to -10 °C, the ARF fell to 1.2.

Table 3. Adhesion reduction factor (ARF) values of samples covered with the PTFE solid lubricant film.

	Pull-Off Force (µN)	WCA (°)	CAH (°)
Aluminum	0.182 ± 0.8	62 ± 5	83 ± 4
PTFE	0.105 ± 0.01	94 ± 2	48 ± 6

3.4. Effect of Roughness on Ice Adhesion

Figure 6 illustrates the maximum adhesive shear force required to detach the ice from bare Al and PTFE solid lubricant samples with various surface roughness values at -10 °C. This temperature was selected since it resulted in the highest adhesion in the previous section of the study. The error bars correspond to the standard deviation of the nine measurements. The ice adhesion shear force was measured at about 130 N for the bare Al and 80 N for the PTFE solid lubricant for substrates with a similar roughness of 0.3 µm. For a higher roughness of 1 µm, the bare Al substrate showed an adhesive shear force of 180 N, and the PTFE solid lubricant showed an adhesive shear force of 130 N.

Therefore, with an increase in the average roughness (R_a) of samples, an increase in the ice shear adhesion of the PTFE solid lubricant and Al was observed. However, for both studied roughness values, the PTFE solid lubricant film demonstrated lower ice adhesion than Al. Regarding ARF, the comparison of substrates with a roughness of 0.3 µm was 1.62, and this value decreased to 1.36 when the average roughness of samples increased to 1 µm.

Comparing the surface roughness based only on the average roughness can be misleading; therefore, the roughness details of PTFE solid lubricant and bare Al samples with identical R_a were measured and are represented in Table 4.
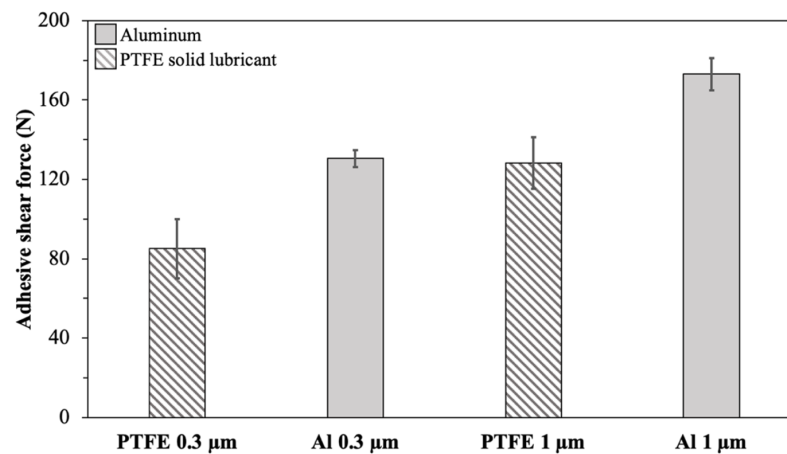
Figure 6. The maximum force of ice detachment for different roughness at −10 °C.

Table 4. Roughness details of PTFE solid lubricant and Al.

	R_a (µm)	R_q (µm)	R_{sk}	R_{ku}
PTFE	1 ± 0.3	1.3 ± 0.4	0.05	4.12
Al	1 ± 0.4	1.6 ± 0.35	0.85	7.04

Table 4 shows that the PTFE solid lubricant sample has a smaller R_q than bare Al, which means the deviation of the average roughness of the PTFE solid lubricant from the mean line is narrower than that of bare Al. In addition, the skewness (R_{sk}) of the PTFE solid lubricant is significantly smaller: with a near-zero skewness; therefore, the PTFE has a symmetrical distribution of peaks and valleys at its surface, while the bare Al surface has a slightly asymmetrical distribution, with slightly more peaks than valleys ($R_{sk} > 0$). Additionally, the height distribution of peaks and valleys on the surface is indicated by the value of R_{ku}, also known as the peakedness of the profile. With an R_{ku} value closer to 3, the surface of the PTFE solid lubricant has a relatively normal peakedness (no outstanding high peaks or deep valleys), while significantly higher values of R_{ku} for Al (7.04) suggest that the surface has comparatively higher peaks and deeper valleys.

3.5. Mechanical Durability Evaluation

To evaluate the durability of the PTFE solid lubricant film, the ice adhesion on PTFE solid lubricant with a 1µm roughness was measured for 25 cycles at −10 °C. Figure 7 shows the average value of ice adhesion of PTFE solid lubricant in every five cycles of icing, and the error bars display the standard deviation of the five measurements that were performed. The solid lubricant film demonstrated acceptable mechanical durability for the first ten cycles showing a 13 percent increase in ice adhesion compared to the first five cycles. Furthermore, by increasing the number of de-icing cycles to 25, the ice shear adhesion of the PTFE solid lubricant was nearly consistent, but the measurement variation rose by 25 percent.

In addition, Figure 8 shows the result of comparing the surface of the PTFE solid lubricant film before (Figure 8a) and at various locations after (Figure 8b) the 25 de-icing cycles to evaluate the mechanical durability of the film. A few black spots were observed on the surface of the PTFE solid lubricant after ice detachment in cycle 25, as shown with red circles in Figure 8b. Although these defects were observed at the front of the sample, a similar phenomenon was not observed in the other three spots of the sample after 25 cycles, as shown in Figure 8b. After multiple de-icing cycles, there was still no trace of film delamination, indicating that the PTFE solid lubricant's adherence to the aluminium substrate was stronger than the measured ice adhesion on the film. Teflon may have suitable bonding with

oxygen on the aluminium surface or in the aluminium oxides on the substrate at the microscopic level.
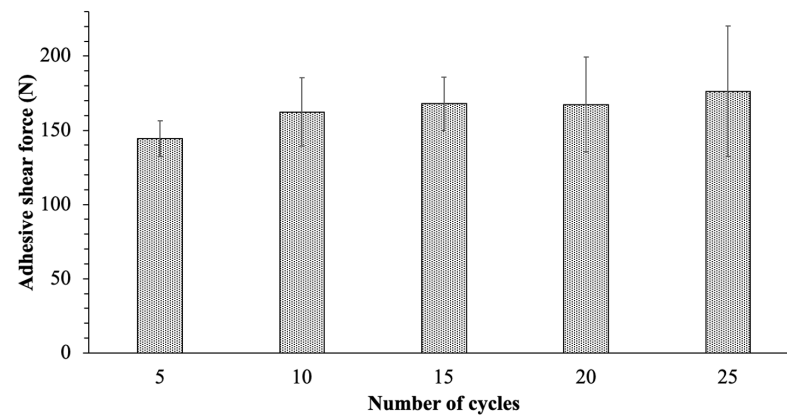

Figure 7. Ice adhesive shear force on the PTFE solid lubricant after differing numbers of de-icing cycles.
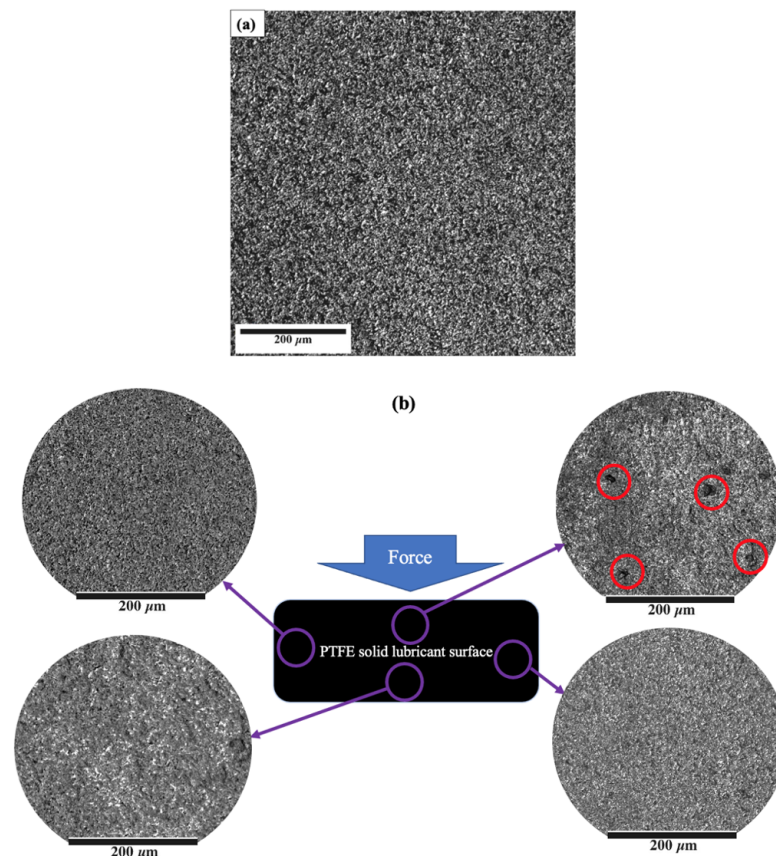

Figure 8. The surface image of the PTFE solid lubricant (**a**) before de-icing, and (**b**) after 25 de-icing cycles at different points of the sample. Possible film detachment is shown by red circles.

4. Discussion

4.1. Ice Behaviour during Detachment

Ice makes noticeably strong contact with the solid substrate when the sample length, Lc, is greater than the threshold value. In this case, interfacial strength is weak, and cracks can propagate at the interface, while in smaller samples, the interface strength is higher, and the failure can be controlled by the crack propagation within the ice [14,57,58]. The

observation of Figure 2c has shown that after increasing the adhesive force, the crack could not grow at the interface and started to propagate through the ice since the interface toughness might be considerably higher than the strength of the ice [57]. Furthermore, the ice was broken into smaller pieces as the shear force increased, which led to distributing the force evenly across the length of each piece, as shown in Figure 2d. It has been shown that stress at the interface is never evenly distributed. When factors such as flaws boost substrate inhomogeneities, it leads to stress concentration, possibly facilitating the crack propagation at the interface of ice and substrate [1,59,60]. Considering $F = \tau \times A$, where τ, assuming the ice interfacial strength is constant, and by decreasing A, the interface area (owing to smaller pieces of ice), a smaller dispersed force per length of contact (F_L) associated with concentrated stress may lead to crack propagation at the interface and ice detached.

As a result, the mechanism for ice detachment on the Al substrate appears to be connected to the ice cracking (cohesive failure) at first, followed by crack propagation, and then the opening and detaching of smaller pieces of ice with increasing shear force. Based on these points, an ice detachment mechanism for bare Al is suggested, as seen in Figure 9. Figure 9a shows the initiation of cracks that happened at the interface of ice and Al at the side and top view. The observations made for crack propagation in Figure 2c are demonstrated schematically in Figure 9b. Finally, the increasing locally applied force as the ice starts fracturing into smaller pieces and detaching (Figure 2d) is represented in Figure 9c. As shown in Figure 2e, failure was fully adhesive since no remnants of the ice were seen on the substrate after total ice detachment [61].
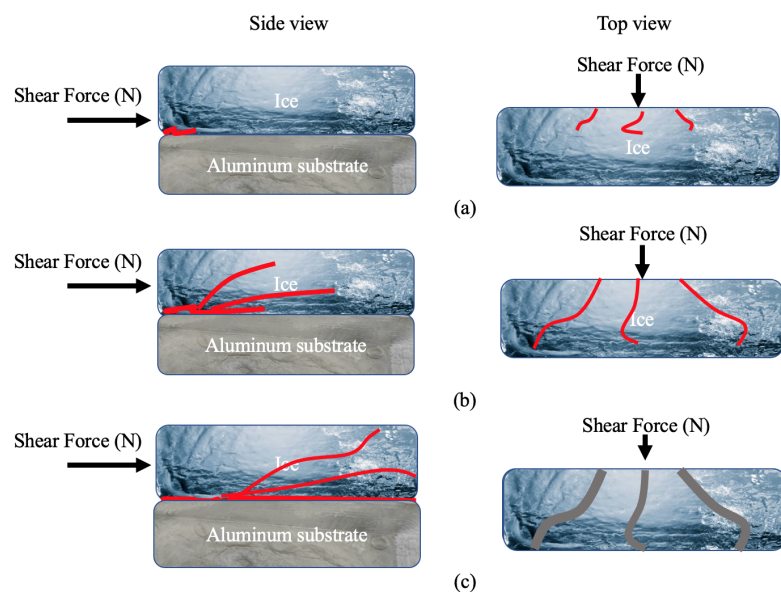

Figure 9. Schematic of ice detachment on bare aluminium, (**a**) crack initiation (side and top view), (**b**) crack propagation (side and top view), and (**c**) wider crack propagation at the interface and ice detachment (side and top view).

The observations for the ice detachment mechanism on PTFE solid lubricant were notably different from bare Al, as observed in Figures 3 and 4 with the appearance of blisters. According to some research, a similar failure mechanism known as "interfacial cavitation"—a surface buckling instability that propagates along the ice–substrate interface as a result of an elastic mismatch between the ice and its substrate—helped to reduce the ice adhesion [51,52].

The blistering mechanism is schematized in Figure 10. As shown in Figure 10a, a level of compressive stress will be formed within the ice while applying a shear force to the ice. Studies have shown that stress—compressive stress in this study—cannot be dispersed uniformly throughout the interface; but rather accumulates at specific points [62,63]. Therefore, when a

shear force gradually increases to remove the ice, a considerable elastic strain in the direction of the applied force might have been produced by concentrated stress due to the significant mismatch in the elastic module between ice and the PTFE solid lubricant [63]. It has been shown that bending strength, which determines the resistance of atmospheric ice to fracture, is the most important mechanical feature of atmospheric ice for ice removal and shedding [47,50]. Subsequently, because of the compressive stress and elastic strain, ice bending and buckling instability, seen as blisters in Figure 3b,c, can be developed under a reasonable amount of tensile stress normal to the interface between the film and the ice (Figure 10b). Since the ice has been constricted, an increase in shear force and elastic strain could cause the concentrated tensile stress at the contact to progressively rise [46]. Therefore, it was observed in Figure 3d,e that the size of blisters rapidly increased by enhancing the shear force per unit area, and each grew and propagated at the interface in the direction of the applied force as schematically shown in Figure 10c. Most of the bubbles were formed at the centre of the samples, which is in agreement with prior studies, where the length of the sample was not considerable [52]. Once blistering became prevalent, through the number of blisters formed and/or the interfacial area they cover, blisters might connect as shown in Figure 3f, immediately producing a pathway for ice detachment to occur from the PTFE solid lubricant.
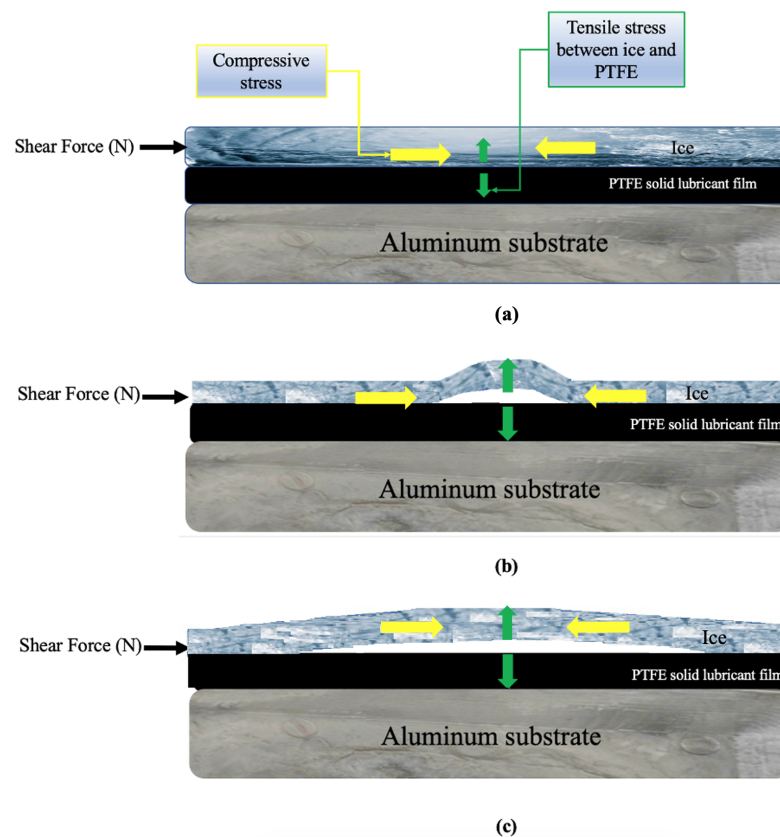

Figure 10. Blistering mechanism at the ice–PTFE solid lubricant interface: (**a**) application of shear force and the formation of compressive stress, (**b**) formation of blisters due to tensile stress at the interface, (**c**) propagation of blisters in the direction of the applied shear force.

4.2. Effect of Icing Temperature

To analyse the effect of icing temperature on ice adhesion, the effect of surface energy (results of Table 2) and icing temperature (Figure 5) should be considered simultaneously. Since Al has a higher wettability compared to the PTFE solid lubricant film (Table 2), water droplets have the potential to fully spread over surfaces and diffuse into surface asperities before freezing at higher temperatures, such as $-2\ ^{\circ}\text{C}$. Consequently, these droplets might make strong bonds with all asperities during freezing and produce strong mechanical interlocking with the substrate [64]. Therefore, this may explain that interfacial toughness

was stronger such that detachment needed more shear force to propagate the crack (as shown in Figure 9) and detach the ice from the bare Al substrate compared to the PTFE solid lubricant, as shown in Figure 5.

It is important to mention that PTFE solid lubricant has a lower thermal diffusivity compared to Al [65,66]. Since lower thermal diffusivity will cause the droplet temperature to reduce more slowly over the same period of time, a higher surface temperature will be measured for the PTFE compared to aluminium. As previously mentioned, the IR camera gave additional evidence that the surface temperature of the PTFE solid lubricant did not immediately decrease and that droplets may remain in the liquid phase on the surface of the PTFE solid lubricant for a longer time after the impact. Furthermore, the droplets might have a smaller contact area with the substrate during freezing since PTFE solid lubricant has a larger WCA and a lower CAH (Table 2) than Al. As a result, the droplets likely make a weaker mechanical interlocking with PTFE solid lubricant when frozen. This could explain why it is easier to separate the formed ice on the PTFE solid lubricant surface compared to Al (Figure 5). Since other studies on atmospheric ice adhesion measured ARF values ranging from 1.2 to 4 [67,68], the results of Table 3 demonstrate the acceptable performance of the PTFE solid lubricant, particularly in the presence of clear ice, which appears at higher temperatures (0 °C to −3 °C) and is considered as the most undesirable type of ice to detach. The gradual decrease in the difference between ice adhesion to the PTFE solid lubricant and Al, with decreasing temperature (Figure 5 at −10 °C), might be due to a decrease in surface temperature of the PTFE solid lubricant. Temperature reduction can reduce the effect of wettability for the PTFE solid lubricant, which can affect the diffusing water droplet into the surface asperities and ice adhesion [69].

As shown in Figure 5, the effect of temperature was more significant on the variation of ice adhesion for the PTFE solid lubricant (40 N to 140 N versus 120 N to 180 N for pure Al). To better understand how temperature affects the ice detachment on the PTFE solid lubricant, the change in ice properties with temperature, notably strength, should be paired with the wettability and water mobility on the film (Table 2). It has been shown that increasing the icing temperature to ambient temperatures increases the ice strength and reduces its bending [50,70]. Additionally, the effect of temperature on the strength of mixed ice is different: it has been demonstrated that an increase in the modulus and strength of rime-mixed ice compared to mixed ice [47,50,71]. In this study, clear or glaze ice, which is more resilient and difficult to strain and bend, could develop at a temperature close to ambient. Due to the higher strength and lower bending of clear ice [46], the production of blisters at the interface of the PTFE solid lubricant and clear ice (as shown in Figure 10b) might be particularly challenging (see smaller blisters in Figure 4a), resulting in a higher shear force to separate the ice. Ice structure can progressively shift from clear ice to the type of ice with a bigger grain size with a weaker structure (mixed) by lowering the temperature, for instance, to −6 °C [32,70]. As mentioned before, the relatively higher surface temperature of the PTFE solid lubricant could lead to a smaller contact area between the liquid water droplet and substrate. A smaller contact area after freezing could possibly have facilitated the formation of a bigger blister at a lower shear force (Figure 4b with mixed ice) compared to the size of blisters in other temperatures (Figure 4a with glaze ice, and Figure 4c with rime-mixed ice). As shown in Figure 4b, a larger blister covered a considerable portion of the interface; ice detachment might have resulted from easier propagation at a lower shear force. By a greater reduction in temperature to −10 °C, the effect of surface energy on wettability could be reduced, as other studies have shown [69], and the contact area between ice and the PTFE solid lubricant might have been increased. Furthermore, the type of ice changes to rime-mixed ice, with higher strength than mixed ice, which could not easily bend. The lower elastic strain rate of ice in lower temperatures and its effect on adhesion has been shown by other studies [52,72,73]. Therefore, the observation of narrow blisters appearing in Figure 4c, which only spread at higher shear strengths, may suggest that a greater shear force would be required to generate more tensile stress at the interface in order to separate the ice.

4.3. Effect of Roughness

A lower ice adhesion of the PTFE solid lubricant compared to Al with similar surface roughness (Figure 6) can also be understood through the correlation between substrate temperature, surface energy, and roughness. It might be challenging to compare the results of rime-mixed ice adhesion because of the complexity of this type of ice and the dependence of its structure, grain size, grain shape, air bubbles, and cavities on the circumstances of accumulation, and the sample position in the accumulated ice, so it seems more reasonable to compare the ARF [50].

The results of other experiments have demonstrated that low surface roughness combined with low surface energy might result in lower ice adhesion [74]. In this study, when water droplets impact the substrate at $-10\ °C$, there will be less surface contact area between water droplets and asperities of the PTFE solid lubricant sample compared to bare Al due to its low surface energy (Table 2) and less significant roughness parameters (Table 4). The results of Figure 6 and previous research [74], which show that the effect of roughness on ice adhesion is lessened by reducing the several roughness parameters, are both in agreement with the possibility that a smaller contact area could have led to lower ice adhesion to the PTFE solid lubricant at $-10\ °C$. Furthermore, a comparison of the obtained ARF values of this study (Table 3), between 1.2 and 3.4, with other experiment values of 2.5 [75], demonstrate the icephobic performance of the PTFE solid lubricant film.

On the other hand, the presence of air pockets at the interface, reported to reduce ice detachment, might be possible during the static ice formation on a textured or rough surface [23]. However, the surface of PTFE solid lubricant has no significant roughness parameters to confirm air pocket entrapment at the interface of ice–film. Additionally, the high-speed impact of the small and supercooled water droplet diffuses to any available pores on the surface that can be filled by air pockets and replaced by ice nucleation. Higher ice adhesion of Al with similar R_a (Figure 6) can be due to its different peak and valley heights and peakedness, based on the results of Table 4. Water droplets could fill the Al surface texture when the surface has greater surface energy (Table 2), and while the surface roughness (R_a) may be similar, different roughness features, such as R_{sk} or R_{ku} (Table 4), could also lead to more droplets filling the Al surface texture compared to the PTFE solid lubricant. Combining high roughness and wettability can result in a significant contact area at the solid–liquid interface upon droplet impact. The strong links between the ice and Al substrate could result from continuous heat exchange between the droplet and the rough surface during freezing [74,76], as well as the suggested mechanical interlocking. Therefore, the required shear force should prevail over a higher interfacial strength between the ice and Al substrate since the interlocking of the ice made detachment more difficult.

In order to analyse the impact of roughness on the blistering mechanism (Figure 3), it is important to note that many studies believed that detachment of ice under similar mechanisms, such as bubble displacement [77] or cavitation propagation [63], is mainly dominated by the difference in the module of elasticity [77], interfacial length [52], and thickness of the film [63]. On the other hand, it has been suggested that a sample with a longer length may be able to clearly demonstrate the influence of roughness, as the effect of length on crack initiation, propagation, and cavitation has been similarly discussed in prior research [52,53,78]. Moreover, there was no significant difference in the number, form, or propagation mode of blisters for the PTFE solid lubricant with varied roughness. The only variation was the force at which blisters formed and spread, which was also noticed when the temperature was changed (Figure 4). Therefore, the reason could be founded on differences in the number and depth of mechanical locking spots when comparing the adhesion of the PTFE solid lubricant with roughnesses of 0.3 μm and 1 μm. A weaker interlocking might have happened at the interface of the ice, which could have facilitated ice detachment when smaller tensile stress might have been needed to form and spread blisters at the ice interface and PTFE solid lubricant film.

4.4. Durability of Solid Lubricant

The PTFE solid lubricant could sustain its icephobic qualities for 20 de-icing cycles and did not show a significant increase in ice shear adhesion for the lowest temperature scenario (−10 °C), as shown in Figure 7. The adhesion variation was increased after 25 cycles of de-icing to values more than ice adhesion on bare Al, which shows the film might have lost its icephobicity. Other studies have shown that this can be due to proper adherence between the PTFE solid lubricant and bare Al, where the asperities of the Al substrate served as an anchor for maintaining the PTFE solid lubricant film [79], therefore preserving the integrity of the film while cycling. Furthermore, some black spots were mostly observed at the front of the sample after ice detachment, shown with red circles in Figure 8b. The front of the sample, where the shear force was applied during the ice detachment, had the highest level of stress concentration, which may indicate some detachment of the PTFE solid lubricant film, therefore, might be the reason for forming black spots, as observed in Figure 8b. However, these defects did not affect the average value of ice adhesion significantly, and only an increase in the variation of the measurements was observed.

5. Conclusions

This study compared the ice adhesion of an environmentally friendly and non-toxic PTFE solid lubricant film on an Al 6061 substrate with the ice adhesion on a bare Al 6061 as a reference. More specifically, the ice shear adhesive force and adhesive reduction factor (ARF) were determined with a custom-built test rig. An icing wind tunnel (IWT) was used to simulate in-flight icing conditions to develop ice with accurate control over the icing parameters. The interfacial mechanism on the PTFE solid lubricant film was determined as the formation of blisters at the centre of the sample, with ensuing propagation toward the edges. By combining the interface analysis and results of the effect of temperature and roughness on the ice adhesion, it was concluded that ice adhesion and interlocking were decreased by the blistering mechanism and lower surface energy of PTFE solid lubricants. More specifically, the ice shear adhesion strength was measured on the PTFE solid lubricant and was compared with bare Al in temperatures ranging from −2 °C to −10 °C. The PTFE solid lubricant helped to decrease the adhesion by about 30 to 50 percent in the considered temperature range. The PTFE solid lubricant performed notably well at −2 °C, where clear ice (as the worst-case scenario) was formed. When surface roughness increased, the ice adhesion strength increased for both substances, and this could be associated with the higher ice–substrate contact area that leads to more mechanical interlocking. After 20 cycles, the PTFE solid lubricant coating showed durable anti-icing performance, but the performance of the film was reduced when increasing the number of de-icing cycles to 25. The results of this investigation provide important insights into the creation of green substitutes that could be able to take the place of unsustainable icephobic coatings in the future.

References

1. Makkonen, L. Ice adhesion—theory, measurements and countermeasures. *J. Adhes. Sci. Technol.* **2012**, *26*, 413–445. [CrossRef]
2. Cober, S.G.; Isaac, G.A. Characterization of aircraft icing environments with supercooled large drops for application to commercial aircraft certification. *J. Appl. Meteorol. Climatol.* **2012**, *51*, 265–284. [CrossRef]

3. Petty, K.R.; Floyd, C.D. A statistical review of aviation airframe icing accidents in the US. In Proceedings of the 11th Conference on Aviation, Range, and Aerospace Hyannis, Hyannis, MA, USA, 4–8 October 2004.

4. Liu, B.; Zhang, K.; Tao, C.; Zhao, Y.; Li, X.; Zhu, K.; Yuan, X. Strategies for anti-icing: low surface energy or liquid-infused? *RSC Adv.* **2016**, *6*, 70251–70260. [CrossRef]

5. Meuler, A.J.; Smith, J.D.; Varanasi, K.K.; Mabry, J.M.; McKinley, G.H.; Cohen, R.E. Relationships between water wettability and ice adhesion. *ACS Appl. Mater. Interfaces* **2010**, *2*, 3100–3110. [CrossRef]

6. Michels, A.; Soave, P.; Nardi, J.; Jardim, P.; Teixeira, S.; Weibel, D.; Horowitz, F. Adjustable, (super) hydrophobicity by e-beam deposition of nanostructured PTFE on textured silicon surfaces. *J. Mater. Sci.* **2016**, *51*, 1316–1323. [CrossRef]

7. Mobarakeh, L.F.; Jafari, R.; Farzaneh, M. Robust icephobic, and anticorrosive plasma polymer coating. *Cold Reg. Sci. Technol.* **2018**, *151*, 89–93. [CrossRef]

8. Wang, Y.; Xue, J.; Wang, Q.; Chen, Q.; Ding, J. Verification of icephobic/anti-icing properties of a superhydrophobic surface. *ACS Appl. Mater. Interfaces* **2013**, *5*, 3370–3381. [CrossRef]

9. Gouni, R. A New Technique to Study Temperature Effects on Ice Adhesion Strength for Wind Turbine Materials. Ph.D. Thesis, Case Western Reserve University, Cleveland, OH, USA, 2011.

10. Work, A.; Lian, Y. A critical review of the measurement of ice adhesion to solid substrates. *Prog. Aerosp. Sci.* **2018**, *98*, 1–26. [CrossRef]

11. Laforte, C.; Blackburn, C.; Perron, J. A review of icephobic coating performances over the last decade. In Proceedings of the SAE 2015 International Conference on Icing of Aircraft, Engines, and Structures, Prague, Czech Republic, 22–25 June 2015.

12. Andersson, L.O. Ice Accretion and Ice Adhesion to Polymer Material. Ph.D. Thesis, Luleå Tekniska Universitet, Lulea, Sweden, 1993.

13. Murase, H.; Nanishi, K. On the relationship of thermodynamic and physical properties of polymers with ice adhesion. *Ann. Glaciol.* **1985**, *6*, 146–149. [CrossRef]

14. Golovin, K.; Kobaku, S.P.; Lee, D.H.; DiLoreto, E.T.; Mabry, J.M.; Tuteja, A. Designing durable icephobic surfaces. *Sci. Adv.* **2016**, *2*, e1501496. [CrossRef]

15. Donadei, V.; Koivuluoto, H.; Sarlin, E.; Vuoristo, P. Lubricated icephobic coatings prepared by flame spraying with hybrid feedstock injection. *Surf. Coatings Technol.* **2020**, *403*, 126396. [CrossRef]

16. Ford, T.; Nichols, O. *Adhesion-Shear Strength of Ice Frozen to Clean and Lubricated Surfaces*; Technical Report; Naval Research Lab: Washington, DC, USA, 1962.

17. Li, B.; Jiang, X.; Wan, H.; Chen, L.; Ye, Y.; Zhou, H.; Chen, J. Fabrication and tribological behaviors of a novel environmental friendly water-based PAI-PTFE-LaF3 bonded solid lubricating composite coating. *Tribol. Int.* **2018**, *121*, 400–409. [CrossRef]

18. Li, B.; Jiang, X.; Wan, H.; Chen, L.; Ye, Y.; Zhou, H.; Chen, J. Environment-friendly aqueous PTFE based bonded solid lubricating coatings: Mechanical and tribological properties under diversified environments. *Prog. Org. Coatings* **2019**, *137*, 104904. [CrossRef]

19. Eshaghi, A.; Mesbahi, M.; Aghaei, A.A. Transparent hierarchical micro-nano structure PTFE-SiO$_2$ nanocomposite thin film with superhydrophobic, self-cleaning and anti-icing properties. *Optik* **2021**, *241*, 166967. [CrossRef]

20. Ghalmi, Z.; Farzaneh, M. Experimental investigation to evaluate the effect of PTFE nanostructured roughness on ice adhesion strength. *Cold Reg. Sci. Technol.* **2015**, *115*, 42–47. [CrossRef]

21. Chang, X.; Li, M.; Tang, S.; Shi, L.; Chen, X.; Niu, S.; Zhu, X.; Wang, D.; Sun, S. Superhydrophobic micro-nano structured PTFE/WO3 coating on low-temperature steel with outstanding anti-pollution, anti-icing, and anti-fouling performance. *Surf. Coat. Technol.* **2022**, *434*, 128214. [CrossRef]

22. Ghalmi, Z.; Farzaneh, M. Durability of nanostructured coatings based on PTFE nanoparticles deposited on porous aluminum alloy. *Appl. Surf. Sci.* **2014**, *314*, 564–569. [CrossRef]

23. Yao, W.; Wu, L.; Sun, L.; Jiang, B.; Pan, F. Recent developments in slippery liquid-infused porous surface. *Prog. Org. Coat.* **2022**, *166*, 106806. [CrossRef]

24. Kim, J.H.; Kim, M.J.; Lee, B.; Chun, J.M.; Patil, V.; Kim, Y.S. Durable ice-lubricating surfaces based on polydimethylsiloxane embedded silicone oil infused silica aerogel. *Appl. Surf. Sci.* **2020**, *512*, 145728. [CrossRef]

25. Yilgor, I.; Bilgin, S.; Isik, M.; Yilgor, E. Facile preparation of superhydrophobic polymer surfaces. *Polymer* **2012**, *53*, 1180–1188. [CrossRef]

26. Yeganehdoust, F.; Amer, A.; Sharifi, N.; Karimfazli, I.; Dolatabadi, A. Droplet mobility on slippery lubricant impregnated and superhydrophobic surfaces under the effect of air shear flow. *Langmuir* **2021**, *37*, 6278–6291. [CrossRef]

27. Chien, C.H.; Chen, T.L.; Wu, X.Y.; Chen, Y.C.; Lee, P.Y.; Lin, L.Y.; Wang, W.L.; Hsueh, H.Y. Bilayer Lubricant-Infused Particulate Films as Slippery Protective Coatings with Durable Anticorrosion and Antifouling Performance. *Adv. Mater. Interfaces* **2022**, *9*, 2102144. [CrossRef]

28. Bart, J.C.; Gucciardi, E.; Cavallaro, S. (Eds.) Lubricants: Properties and Characteristics. In *Biolubricants Science and Technology*; Woodhead Publishing Ltd.: Cambridge, UK, 2013; pp. 24–73.

29. Czarny, R.; Paszkowski, M. The influence of graphite solid additives, MoS2 and PTFE on changes in shear stress values in lubricating greases. *J. Synth. Lubr.* **2007**, *24*, 19–29. [CrossRef]

30. Dubey, M.K.; Bijwe, J.; Ramakumar, S. PTFE based nano-lubricants. *Wear* **2013**, *306*, 80–88. [CrossRef]

31. Stachowiak, G.W.; Batchelor, A.W. *Engineering Tribology*; Butterworth-Heinemann: Oxford, UK, 2013.

32. Rønneberg, S.; Laforte, C.; Volat, C.; He, J.; Zhang, Z. The effect of ice type on ice adhesion. *AIP Adv.* **2019**, *9*, 055304. [CrossRef]

33. Jeong, M. *Ice Shear Adhesion Strength Measurement Techniques*; Mechanical & Aerospace Engineering Department, University of Virginia: Charlottesville, VA, USA, 2020; pp. 2–16.
34. Riahi, M.M.; Marceau, D.; Laforte, C.; Perron, J. The experimental/numerical study to predict mechanical behaviour at the ice/aluminium interface. *Cold Reg. Sci. Technol.* **2011**, *65*, 191–202. [CrossRef]
35. Mittal, K. Adhesion measurement of thin films. *Electrocompon. Sci. Technol.* **1976**, *3*, 21–42. [CrossRef]
36. Strobl, T.; Raps, D.M.; Hornung, M. Evaluation of roughness effects on ice adhesion. In Proceedings of the 5th AIAA Atmospheric and Space Environments Conference, San Diego, CA, USA, 24–27 June 2013; p. 2547.
37. *ISO 4288:1996*; Geometrical Product Specifications (GPS)–Surface Texture: Profile Method–Rules and Procedures for the Assessment of Surface Texture. ISO: Geneva, Switzerland, 1996.
38. Gadelmawla, E.; Koura, M.M.; Maksoud, T.M.; Elewa, I.M.; Soliman, H. Roughness parameters. *J. Mater. Process. Technol.* **2002**, *123*, 133–145. [CrossRef]
39. Adams, G.G. Adhesion and pull-off force of an elastic indenter from an elastic half-space. *Proc. R. Soc. A Math. Phys. Eng. Sci.* **2014**, *470*, 20140317. [CrossRef]
40. Sharifi, N.; Pugh, M.; Moreau, C.; Dolatabadi, A. Developing hydrophobic and superhydrophobic TiO_2 coatings by plasma spraying. *Surf. Coat. Technol.* **2016**, *289*, 29–36. [CrossRef]
41. Kulinich, S.; Farzaneh, M. How wetting hysteresis influences ice adhesion strength on superhydrophobic surfaces. *Langmuir* **2009**, *25*, 8854–8856. [CrossRef] [PubMed]
42. Stalder, A.F.; Melchior, T.; Müller, M.; Sage, D.; Blu, T.; Unser, M. Low-bond axisymmetric drop shape analysis for surface tension and contact angle measurements of sessile drops. *Colloids Surf. Physicochem. Eng. Asp.* **2010**, *364*, 72–81. [CrossRef]
43. De Pauw, D.; Dolatabadi, A. Effect of superhydrophobic coating on the anti-icing and deicing of an airfoil. *J. Aircr.* **2017**, *54*, 490–499. [CrossRef]
44. Puffing, R.F.; Peciar, M.; Hassler, W. Instrumentation of an Icing Wind Tunnel Based on SAE Standards. *Sci. Proc. Fac. Mech. Eng. Slovak Univ. Technol. Bratisl.* **2013**, *21*, 37. [CrossRef]
45. Chen, T.; Cong, Q.; Sun, C.; Jin, J.; Choy, K.L. Influence of substrate initial temperature on adhesion strength of ice on aluminum alloy. *Cold Reg. Sci. Technol.* **2018**, *148*, 142–147. [CrossRef]
46. Druez, J.; Nguyen, D.; Lavoie, Y. Mechanical properties of atmospheric ice. *Cold Reg. Sci. Technol.* **1986**, *13*, 67–74. [CrossRef]
47. Kermani, M.; Farzaneh, M. Flexural and low-cycle fatigue behavior of atmospheric ice. *J. Mater. Sci.* **2009**, *44*, 2497–2506. [CrossRef]
48. Druez, J.; Phan, C.; Laforte, J.; Nguyen, D. The adhesion of glaze and rime on aluminium electrical conductors. *Trans. Can. Soc. Mech. Eng.* **1978**, *5*, 215–220. [CrossRef]
49. Chu, M.; Scavuzzo, R. Adhesive shear strength of impact ice. *AIAA J.* **1991**, *29*, 1921–1926. [CrossRef]
50. Kermani, M.; Farzaneh, M.; Gagnon, R. Compressive strength of atmospheric ice. *Cold Reg. Sci. Technol.* **2007**, *49*, 195–205. [CrossRef]
51. Chaudhury, M.; Kim, K. Shear-induced adhesive failure of a rigid slab in contact with a thin confined film. *Eur. Phys. J. E* **2007**, *23*, 175–183. [CrossRef]
52. Mohseni, M.; Dijvejin, Z.A.; Golovin, K. Designing scalable elastomeric anti-fouling coatings: Shear strain dissipation via interfacial cavitation. *J. Colloid Interface Sci.* **2021**, *589*, 556–567. [CrossRef]
53. Dhyani, A.; Choi, W.; Golovin, K.; Tuteja, A. Surface design strategies for mitigating ice and snow accretion. *Matter* **2022**, *5*, 1423–1454. [CrossRef]
54. Law, K.Y. Definitions for hydrophilicity, hydrophobicity, and superhydrophobicity: Getting the basics right. *J. Phys. Chem. Lett.* **2014**, *5*, 686–688. [CrossRef]
55. Israelachvili, J.N. *Intermolecular and Surface Forces*; Academic Press: Washington, DC, USA, 2011.
56. Alizadeh, A.; Yamada, M.; Li, R.; Shang, W.; Otta, S.; Zhong, S.; Ge, L.; Dhinojwala, A.; Conway, K.R.; Bahadur, V.; et al. Dynamics of ice nucleation on water repellent surfaces. *Langmuir* **2012**, *28*, 3180–3186. [CrossRef]
57. Zarasvand, K.A.; Mohseni, M.; Golovin, K. Cohesive zone analysis of cylindrical ice adhesion: Determining whether interfacial toughness or strength controls fracture. *Cold Reg. Sci. Technol.* **2021**, *183*, 103219. [CrossRef]
58. Golovin, K.; Dhyani, A.; Thouless, M.; Tuteja, A. Low–interfacial toughness materials for effective large-scale deicing. *Science* **2019**, *364*, 371–375. [CrossRef]
59. Subramanyam, S.B.; Rykaczewski, K.; Varanasi, K.K. Ice adhesion on lubricant-impregnated textured surfaces. *Langmuir* **2013**, *29*, 13414–13418. [CrossRef]
60. Nosonovsky, M.; Hejazi, V. Why superhydrophobic surfaces are not always icephobic. *ACS Nano* **2012**, *6*, 8488–8491. [CrossRef]
61. Andrews, E.; Lockington, N. The cohesive and adhesive strength of ice. *J. Mater. Sci.* **1983**, *18*, 1455–1465. [CrossRef]
62. Laforte, C.; Laforte, J.L. Deicing strains and stresses of iced substrates. *J. Adhes. Sci. Technol.* **2012**, *26*, 603–620. [CrossRef]
63. Wang, C.; Fuller, T.; Zhang, W.; Wynne, K.J. Thickness dependence of ice removal stress for a polydimethylsiloxane nanocomposite: Sylgard 184. *Langmuir* **2014**, *30*, 12819–12826. [CrossRef]
64. Cao, Y.; Tan, W.; Wu, Z. Aircraft icing: An ongoing threat to aviation safety. *Aerosp. Sci. Technol.* **2018**, *75*, 353–385. [CrossRef]
65. Choi, C.H.; Mittal, K. *Ice Adhesion: Mechanism, Measurement, and Mitigation*; John Wiley & Sons: New York, NY, USA, 2020.
66. Liu, X.; Chen, H.; Zhao, Z.; Yan, Y.; Zhang, D. Slippery liquid-infused porous electric heating coating for anti-icing and de-icing applications. *Surf. Coat. Technol.* **2019**, *374*, 889–896. [CrossRef]

67. Kulinich, S.; Farzaneh, M. Ice adhesion on super-hydrophobic surfaces. *Appl. Surf. Sci.* **2009**, *255*, 8153–8157. [CrossRef]

68. Momen, G.; Jafari, R.; Farzaneh, M. Ice repellency behaviour of superhydrophobic surfaces: Effects of atmospheric icing conditions and surface roughness. *Appl. Surf. Sci.* **2015**, *349*, 211–218. [CrossRef]

69. Ou, J.; Shi, Q.; Wang, Z.; Wang, F.; Xue, M.; Li, W.; Yan, G. Sessile droplet freezing and ice adhesion on aluminum with different surface wettability and surface temperature. *Sci. China Phys. Mech. Astron.* **2015**, *58*, 1–8. [CrossRef]

70. Schulson, E.; Lim, P.; Lee, R. A brittle to ductile transition in ice under tension. *Philos. Mag. A* **1984**, *49*, 353–363. [CrossRef]

71. Jones, S.J.; Chew, H. Effect of sample and grain size on the compressive strength of ice. *Ann. Glaciol.* **1983**, *4*, 129–132. [CrossRef]

72. Douglass, R.G.; Palacios, J.L. Effects of strain rate variation on the shear adhesion strength of impact ice. *Cold Reg. Sci. Technol.* **2021**, *181*, 103168. [CrossRef]

73. Wenyuan, M.; Yingkui, G. Experimental study on mechanical properties of ice. In Proceedings of the AASRI International Conference on Industrial Electronics and Applications (IEA 2015), London, UK, 27–28 June 2015; Atlantis Press: Paris, France, 2015; pp. 192–196.

74. Bharathidasan, T.; Kumar, S.V.; Bobji, M.; Chakradhar, R.; Basu, B.J. Effect of wettability and surface roughness on ice-adhesion strength of hydrophilic, hydrophobic and superhydrophobic surfaces. *Appl. Surf. Sci.* **2014**, *314*, 241–250. [CrossRef]

75. Menini, R.; Farzaneh, M. Elaboration of Al_2O_3/PTFE icephobic coatings for protecting aluminum surfaces. *Surf. Coatings Technol.* **2009**, *203*, 1941–1946. [CrossRef]

76. Memon, H.; Liu, J.; De Focatiis, D.S.; Choi, K.S.; Hou, X. Intrinsic dependence of ice adhesion strength on surface roughness. *Surf. Coat. Technol.* **2020**, *385*, 125382. [CrossRef]

77. Beemer, D.L.; Wang, W.; Kota, A.K. Durable gels with ultra-low adhesion to ice. *J. Mater. Chem. A* **2016**, *4*, 18253–18258. [CrossRef]

78. Golovin, K.; Tuteja, A. A predictive framework for the design and fabrication of icephobic polymers. *Sci. Adv.* **2017**, *3*, e1701617. [CrossRef]

79. Soltani-Kordshuli, F.; Okyere, D.; Chen, J.; Miller, C.; Harris, N.; Afshar-Mohajer, M.; Ghosh, S.K.; Zou, M. Tribological behavior of the PDA/PTFE+ Cu-SiO_2 nanoparticle thin coatings. *Surf. Coat. Technol.* **2021**, *409*, 126852. [CrossRef]